DOI: 10.1002/chem.200800886

Understanding the Two-Step Spin-Transition Phenomenon in Iron(II) 1D Chain Materials

Suzanne M. Neville,*[a] Benjamin A. Leita,[a] Gregory J. Halder,[b, c] Cameron J. Kepert,[b] Boujemaa Moubaraki,[a] Jean-François Létard,[d] and Keith S. Murray*[a]

Abstract: Three analogous one dimensional (1D) polymeric iron(II) spin crossover (SCO) materials containing the new ligand 4,6-bis(2′,2″-pyridyl)pyrazine (bdpp) have been comprehensively characterised magnetically (thermal and light-induced) and structurally. Within this series are two polymorphs of the formula $[Fe(NCS)_2(bdpp)]$, **1** and **2a**, which differ magnetically in that phase **1** undergoes a full two-step SCO ($T_{1/2(1)}=135$ K and $T_{1/2(2)}=90$ K) whereas phase **2a** remains high spin (HS) over all temperatures. The central distinction between these two materials lies in the presence of intermolecular π–π interactions generated by the crystal packing in **1**, which are absent in **2a**. The isostructural selenocyanate analogue of **2a**, $[Fe(NCSe)_2(bdpp)]$, **2b**, undergoes a full two-step SCO ($T_{1/2(1)}=200$ K and $T_{1/2(2)}=125$ K). Structural analyses of **1** and **2b** at a range of temperatures provide deep insight into their two-step SCO nature. Structural analysis of **1** at 25 K ($\mathbf{1}^{LS-LS}$), 123 K ($\mathbf{1}^{LS-HS}$) and 250 K ($\mathbf{1}^{HS-HS}$) reveals two distinct iron(II) centres at each temperature, with ordered, alternating HS and LS (low spin) sites at the intermediate plateau (IP) temperatures. In contrast, structural analysis of **2b** at 90 K ($\mathbf{2b}^{LS}$), 150 K ($\mathbf{2b}^{LS/HS}$) and 250 K ($\mathbf{2b}^{HS}$) reveals one unique iron(II) centre at each temperature with an "averaged" LS/HS character at the IP temperature. Weak planes of diffuse scattering in the single-crystal X-ray diffraction patterns were observed for this phase at 90 and 150 K, indicating that 1D long range ordering of alternating HS/LS iron(II) centres occurs along the 1D coordination chains, but that there is no correlation between chains. The lack of observable diffuse scattering at 250 K suggests that the onset of the 1D structural ordering in the chain direction corresponds to the first step of the SCO and that this structural transition is electronically driven. The photomagnetic properties of both **1** and **2b** have been investigated and show ≈62 and 53% photo-excitation of a HS metastable state at low temperatures and T(LIESST) values of 55 and 49 K, respectively. Relaxation studies on the HS fraction in **2b** fitted well to a stretched exponential model with kinetic parameters indicative of weak cooperativity.

Keywords: 1D chain · chain structures · iron · magnetic properties · spin crossover

Introduction

Spin crossover (SCO), an electronic switching phenomenon that can occur in d^4–d^7 transition metals, has been the subject of intense investigation over recent decades towards developing materials for applications as molecular binary switches and electronic data storage devices.[1,2] These applications stem from the dramatic magnetic and physical changes detectable over the transition between high-spin (HS; $S=2$ for d^6) and low-spin (LS; $S=0$ for d^6) states (through temperature, pressure or light-irradiation).[1,2] Of particular interest are SCO materials that display bistability (i.e. the existence of two electronic states under the same perturbation) thus inducing a memory effect. It is well established that the SCO effect is propagated in the solid state by strong communication pathways through intermolecular

[a] Dr. S. M. Neville, Dr. B. A. Leita, Dr. B. Moubaraki, Prof. K. S. Murray
School of Chemistry, Monash University
Building 23, Clayton, VIC 3800 (Australia)
Fax: (+61) 3-9905-4597
E-mail: keith.murray@sci.monash.edu.au

[b] Dr. G. J. Halder, Prof. C. J. Kepert
School of Chemistry, The University of Sydney
NSW 2006 (Australia)

[c] Dr. G. J. Halder
Materials Science Division, Argonne National Laboratory
Argonne, Illinois, 60439 (USA)

[d] Dr. J.-F. Létard
Laboratoire des Sciences Moléculaires
ICMCB (CNRS UPR 9048), Université Bordeaux I
33608 Pessac (France)

Supporting information for this article is available on the WWW under http://dx.doi.org/10.1002/chem.200800886.

interactions, such as hydrogen bonding and π stacking.[1,3,4] An alternate approach is to directly link SCO centres in coordinatively-bridged networks, thus further enhancing communication between SCO sites.[5] Indeed, examples of 1-, 2- and 3D SCO polymers exist that show significant communication in the form of abrupt spin transitions with hysteresis.[6–8] Contrasting these are polymeric SCO materials in which flexible linking ligands have been used, which have largely tended to show little cooperativity and, indeed, may even have reduced communication as a consequence of being incorporated into frameworks that are able to flex locally in response to SCO.[9]

Discrete molecular and framework systems that display two-step SCO transitions are of particular interest in that they allow investigation of the influence of SCO on neighbouring metal centres through cooperative/anticooperative intra- and inter-molecular interactions. In the case of dinuclear SCO systems, a small number of phases in which the influence on two-step properties of intramolecular communication between the metal centres and crystal packing have been investigated.[10–12] Such investigations are also important in polymeric 1D systems, such as those presented here in which individual chains may order in the two-step plateau region, for example, HS-LS-HS-LS, or show random disorder. There are three structural cases that have been reported for mononuclear, dinuclear and polynuclear materials that display two-step (or multistep) spin transitions. The most common among these are systems that have multiple crystallographically distinct metal centres at all temperatures; here, the often subtle difference in coordination geometry between different SCO centres is likely the most significant cause of the multiple SCO steps, rather than anticooperative effects between metal centres.[7,8,13,14] Secondly, a number of cases have been reported in which one crystallographically unique metal centre is reported over all temperatures, with an intermediate M–L bond length seen at the IP temperature, owing to random disorder of the HS/LS species at the IP temperature.[15–17] Lastly, and by far the least common, are materials that undergo structural phase transitions associated with one or both of the SCO steps; known examples here include systems in which a single HS iron(II) site at high temperature converts to two sites upon cooling through the first step.[12,18,19] Given the likelihood that at least short-range ordering rather than random disorder of HS-LS sites should exist in the IP region, members of the second family of systems are most likely mis-categorised and belong instead to one of the other two classes. Only recently have structural methods towards exploring these phenomena in detail been available, owing to improved X-ray sources and detectors. Indeed, in recent years there have been additional reports of SCO materials reported nearly 20 years ago that identify new facets of their SCO behaviour previously unexplored or not recognised.[18] To this end, detailed magnetic and structural analyses of SCO materials and comparisons between related systems are essential to decouple the various structural influences on SCO behaviour.

Of a wide range of different SCO systems known, the most predominant are those based on the $[Fe^{II}(NCS)_2(py)_4]$ centre, in which py is any pyridyl donor ligand. Of interest here is the $[Fe^{II}(NCS)_2(dpa)_2]$ coordination environment (a subclass of the $[Fe^{II}(NCS)_2(py)_4]$ family in which dpa is any 2,2′-dipyridyl amine donor ligand), for which mononuclear,[20,21] dinuclear[10,21] and polynuclear 1D chain[22,23] SCO materials have been reported. Despite having similar coordination environments, this family of materials displays diverse SCO behaviours, from one-step and two-step to incomplete.[10,20–23] Detailed structural analyses within these systems have revealed fundamental structural features that account for such varied magnetic behaviours. For example, at the IP temperature for the two-step SCO in the dinuclear compound $[Fe^{II}(NCS)_2(ddpp)]_2{\cdot}4(CH_2Cl_2)$ (ddpp = 2,5-(di-2-pyridylamine)pyridine), an ordering of the [HS-LS] states was observed, the first of its kind.[10] This ordering, and the presence of a two-step SCO, was attributed to the existence of inequivalent iron(II) sites at all temperatures. In a further example, structural analysis of two polymorphs of $[Fe^{II}(NCS)_2(cddt)]_2{\cdot}$(guest) (cddt = 2-chloro-4,6-bis(di-2-pyridylamine)-1,3,5-triazine), which show very different SCO behaviours (one showing an incomplete SCO and the other remaining HS), revealed an array of π–π interactions in the former contributing to the observed SCO.[22] Thus, magneto-structural analysis of further examples within this series is important to gain greater insight into the fundamentals of the SCO phenomenon and, indeed, the two-step conversion process.

We focus here on a new dpa-containing ligand, 4,6-bis(2′,2″-dipyridylamine)pyrimidine (bdpp, Figure 1), which was inspired by our recent work with the related ligand

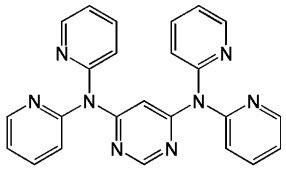

Figure 1. 4,6-Bis(2′,2″-di-pyridylamine)pyrimidine (bdpp).

ddpp. In the dinuclear system $[Fe(NCS)_2(ddpp)]_2{\cdot}4(CH_2Cl_2)$, the pyridine nitrogen atoms coordinate to and bridge the iron(II) centres.[10] In the present systems, by contrast, the pyrimidine rings of the bdpp ligand remain unbound, resulting in the formation of extended polynuclear 1D systems with the general formula $[Fe^{II}(NCX)_2(bdpp)_2]$ (X = S and Se). Through detailed magnetic (thermal and light-induced) and structural analyses of this series of materials we draw detailed relationships between their differing structures and diverse resulting SCO behaviours.

Results

Magnetic susceptibility studies of thermally induced SCO: Magnetic susceptibility measurement was used to follow the iron(II) spin state changes for polycrystalline samples of **1**, **2a** and **2b** (Figure 2 and Figure 3; see the Supporting Information for **2a**). Both **1** and **2b** show a complete two-step SCO although **2a** remains HS overall temperatures with a slight decrease in magnetic response below 15 K, owing to a combination of weak antiferromagnetic coupling and zero-field splitting.

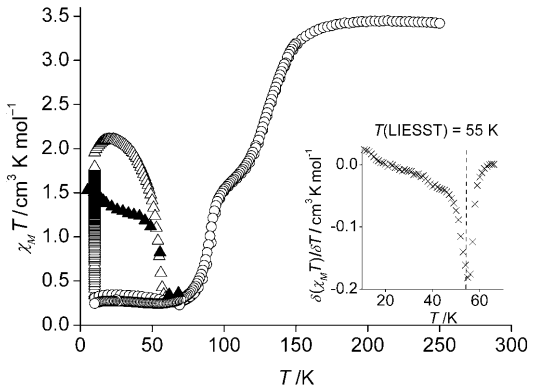

Figure 2. Plot of $\chi_M T$ versus temperature over the range 10–250 K for the thermal and photomagnetic effect for **1** (○: thermal spin transition, ▲: thermal trapping with quench cooling, △: irradiation $\lambda = 512$ nm followed by relaxation). Inset: Plot of $\delta\chi_M T/\delta T$ versus temperature indicating T(LIESST) value of 55 K at the minima.

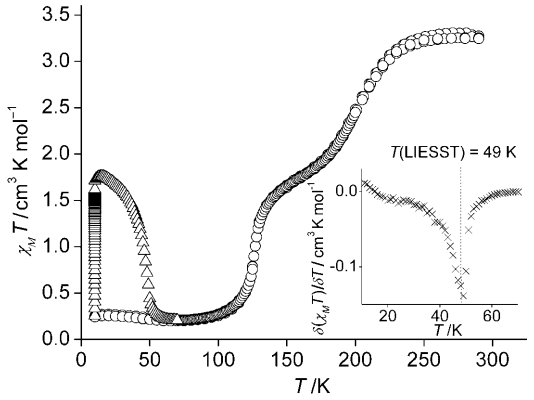

Figure 3. Plot of $\chi_M T$ versus temperature over the range 10–280 K for the thermal and photomagnetic effect for **2b** (○: thermal spin transition, △: irradiation $\lambda = 512$ nm followed by relaxation). Inset: Plot of $\delta\chi_M T/\delta T$ versus temperature indicating T(LIESST) value of 49 K at the minima.

The $\chi_M T$ values for **1** remained approximately constant at 3.45 $cm^3 mol^{-1} K$ between 200 and 250 K, indicative of HS iron(II) (Figure 2). Between 200 and 110 K, the $\chi_M T$ values rapidly decreased to attain a minimum value of 1.73 $cm^3 mol^{-1} K$, indicating that half of the iron(II) sites are in the HS state. The $T_{1/2(1)}$ value of this step is 135 K. Below 110 K, the $\chi_M T$ values decreased, gradually then more rapidly, to attain a minimum value of 0.25 $cm^3 mol^{-1} K$ at 60 K, indicative of iron(II) in the LS state. The $T_{1/2(2)}$ value of this step is 90 K. Below 60 K, the $\chi_M T$ values remained approximately constant. The non-zero magnitude of $\chi_M T$ at low temperature is a common occurrence for iron(II) LS sites and is likely due to second order Zeeman effects. Thermal hysteresis was not observed in the $\chi_M T$ values upon heating. However, upon quench cooling to 4 K thermal trapping of the LS species in the HS state was observed to a maximum of value 1.54 $cm^3 mol^{-1} K$ at 5 K, which corresponds to 43.5 % of the HS iron(II) sites. With heating above 4 K the HS trapped sites gradually decreased to attain a LS state at 60 K. The T(TIESST) value (TIESST = thermally induced excited spin state trapping), defined as the minimum of the $d\chi_M T/dT$ versus T curve is 55 K.[24]

The $\chi_M T$ values for **2b** remained approximately constant at 3.23 $cm^3 mol^{-1} K$ above 250 K, indicative of iron(II) in the HS state (Figure 3). Over the range 250–150 K the $\chi_M T$ values rapidly decreased to a minimum of 1.66 $cm^3 mol^{-1} K$ at 150 K, indicating half of the iron(II) sites are in the HS state. The $T_{1/2(1)}$ value of this step is 200 K. Below 150 K the $\chi_M T$ values decreased, gradually then more rapidly, to attain a minimum of 0.21 $cm^3 mol^{-1} K$ at 80 K, which is indicative iron(II) sites in the LS state. The $T_{1/2(2)}$ value of this step is 125 K. The $\chi_M T$ values remained approximately constant below 80 K. Thermal hysteresis was not observed in the $\chi_M T$ values, nor was any thermal trapping of HS sites observed upon quench cooling.

Magnetic susceptibility studies of light-induced SCO: Materials that show TIESST are also likely to show light-induced excited spin state trapping (LIESST) at low temperatures;[24] hence we followed the magnetic response to **1** upon irradiation with green light (Figure 2). Magnetic susceptibility studies on a thin layer of **1**, irradiated at 10 K showed an increase in the magnetic signal to a maximum $\chi_M T$ value of 1.78 $cm^3 mol^{-1} K$. With further heating above 10 K, in the absence of irradiation, the $\chi_M T$ values increased slightly to a maximum, at 15 K, of 2.13 $cm^3 mol^{-1} K$. This temperature independent increase is due to zero-field splitting of the HS iron(II) centres and was also observed over the same temperature range for thermal SCO described above. This corresponds to 62 % of the iron(II) sites trapped in the metastable HS state, which is increased compared to the 43.5 % attained by quench cooling. With further heating the light-induced metastable HS sites relax to a minimum $\chi_M T$ value of 0.27 $cm^3 mol^{-1} K$ at 60 K, the same temperature at which the thermally induced trapping of iron(II) HS sites was erased. With further heating the $\chi_M T$ values followed the same path as that of the original thermal SCO. The T(LIESST) value, defined as the minimum of the $\delta\chi_M T/\delta T$ versus T curve in the absence of irradiation, for **1** is 55 K (inset: Figure 2).[24]

Despite there being no HS trapping upon quench cooling to low temperatures for **2b**, this does not preclude the existence of the LIESST effect. Indeed, irradiation to a thin layer of **2b** at 10 K resulted in an increase in $\chi_M T$ values to

a maximum of 1.63 $cm^3 mol^{-1} K$. With further heating to ≈15 K, in the absence of irradiation, the magnetic response is temperature independent (as for **1**) with the $\chi_M T$ values attaining a maximum of 1.79 $cm^3 mol^{-1} K$. This corresponds to a maximum of ≈53% of the iron(II) sites in the HS state. With further heating the light-induced iron(II) metastable HS sites relaxed to attain a minimum $\chi_M T$ value of 0.23 $cm^3 mol^{-1} K$ by 60 K. With further heating above 60 K, the magnetic response followed the same path as that of the original thermal SCO. The *T*(LIESST) value for **2b** is 49 K (inset: Figure 3).[24]

Relaxation studies of the HS molar fraction generated by laser irradiation were performed on **2b**. The data, at 10, 40, 46, 50 and 55 K, are shown in Figure 4. The kinetics were

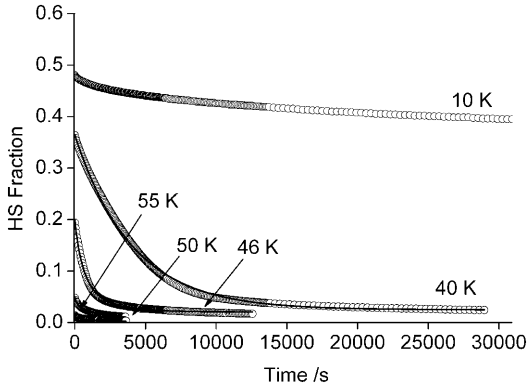

Figure 4. Plot of HS fraction versus time on **2b** for the relaxation kinetics (10, 40, 46, 50 , 55 K) of the light induced metastable HS state. Data were analysed using a stretched exponential treatment: $E_a = 165\ cm^{-1}$, $k_\infty = 0.14\ s^{-1}$ and with a gaussian distribution $\sigma = 40\ cm^{-1}$.

analysed using a stretched exponential treatment to give a very good fit between 55–40 K using the parameters; $E_a = 165\ cm^{-1}$, $k_\infty = 0.14\ s^{-1}$ with a Gaussian distribution $\sigma = 40\ cm^{-1}$. E_a is the apparent activation energy and k_∞ the apparent pre-exponential factor of the activated region. These parameters, together with $k_o = 1.5 \times 10^{-4}\ s^{-1}$ (the overestimated limit of the tunnelling rate constant), were also used to confirm the stretched exponential model and simulate the *T*(LIESST) experimental curve given in Figure 3; the best fit curve, is very good and is shown in the Supporting Information. The use of a stretched exponential, and the low value of the activation energy, E_a, is in agreement with low cooperativity in **2b** (presumably likewise in **1**).

Structural analysis by single-crystal X-ray diffraction: Full single-crystal X-ray diffraction structure and refinement details for $\mathbf{1}^{LS-LS}$, $\mathbf{1}^{LS-HS}$, $\mathbf{1}^{HS-HS}$, **2a**, $\mathbf{2b}^{LS}$, $\mathbf{2b}^{LS/HS}$ and $\mathbf{2b}^{HS}$ are given in Table 1 and selected bond lengths and structural parameters are reported in Table 2. The average Fe–N distance, $\langle d_{Fe-N} \rangle$, octahedral distortion parameter, Σ, and other relevant geometric parameters have been calculated for each of the materials and are presented in Table 2. The $\langle d_{Fe-N} \rangle$ parameter is useful for quantifying the iron(II) spin state. The Σ parameter (defined as the sum of the deviation of each of the 12 *cis*-angles associated with the iron(II) centre) is useful to further quantify the changes in iron(II) environment associated with the SCO, whereby a smaller value is indicative of stabilisation of the LS state.[25]

For each of these materials, structural analysis revealed a distorted octahedral iron(II) environment consisting of two axially coordinated NCS^- or $NCSe^-$ ligands and two equatorially coordinated bis-bidentate bdpp ligands, bound through the terminal di-(2-pyridyl)amine pyridyl group. Each bdpp ligand bridges two iron(II) centres and thus propagates to form extended 1D chains (Figures 5 and 6). Even though these materials are isotopological, the packing of 1D chains in the crystal lattice results in a large variation in crystal symmetry and interactions between adjacent chains and more subtle variation in iron(II) geometry.

*Structure of [Fe(NCS)$_2$(bdpp)] (**1**)*: The complex **1** crystallises in triclinic symmetry and has two crystallographically

Table 1. Single-crystal diffraction data and parameters for $\mathbf{1}^{LS-LS}$, $\mathbf{1}^{LS-HS}$, $\mathbf{1}^{HS-HS}$, **2a**, $\mathbf{2b}^{LS}$, $\mathbf{2b}^{LS/HS}$ and $\mathbf{2b}^{HS}$.

Compound	$\mathbf{1}^{LS-LS}$	$\mathbf{1}^{LS-HS}$	$\mathbf{1}^{HS-HS}$	**2a**	$\mathbf{2b}^{LS}$	$\mathbf{2b}^{LS/HS}$	$\mathbf{2b}^{HS}$
Fe^{II} Spin States (Fe1–Fe2 or Fe1)	LS-LS	LS-HS	HS-HS	HS	LS	LS/HS	HS
T [K]	25	123	250	123	90	150	250
formula	$FeS_2C_{26}H_{18}N_{10}$	$FeS_2C_{26}H_{18}N_{10}$	$FeS_2C_{26}H_{18}N_{10}$	$FeS_2C_{26}H_{18}N_{10}$	$FeSe_2C_{26}H_{18}N_{10}$	$FeSe_2C_{26}H_{18}N_{10}$	$FeSe_2C_{26}H_{18}N_{10}$
M_r [g mol^{-1}]	590.47	590.47	590.47	590.47	684.27	684.27	684.27
space group	triclinic ($P\bar{1}$)	triclinic ($P\bar{1}$)	triclinic ($P\bar{1}$)	monoclinic (*C*2/*c*)	monoclinic (*C*2/*c*)	monoclinic (*C*2/*c*)	monoclinic (*C*2/*c*)
a [Å]	8.564(3)	8.6670(4)	8.6540(2)	23.291(5)	23.2609(10)	23.314(5)	23.5214(17)
b [Å]	8.675(3)	8.7207(4)	8.9690(2)	8.6179(17)	8.5716(4)	8.6078(17)	8.6481(6)
c [Å]	17.473(5)	17.4947(9)	17.5736(5)	17.602(4)	17.6735(8)	17.780(4)	18.0485(15)
α [°]	95.446(5)	95.686(2)	96.838(2)	90	90	90	90
β [°]	103.984(4)	103.610(2)	103.784(2)	126.14(3)	126.434(2)	126.40(3)	126.792(4)
γ [°]	96.526(5)	95.517(2)	94.360(2)	90	90	90	90
V [Å^3]	1241.4(7)	1269.04(11)	1307.59(6)	2853.2(15)	2835.0(2)	2872.0(15)	2940.1(4)
ρ_{calcd} [Mg m^{-3}]	1.580	1.545	1.500	1.375	1.603	1.583	1.546
μ [mm^{-1}]	0.815	0.797	0.774	0.709	3.135	3.094	3.023
$R(F)$ [$I > 2\sigma(I)$]	0.0496	0.0733	0.0452	0.0852	0.1124	0.1064	0.0949
$R(F)$ (all data)	0.0744	0.0758	0.0488	0.1444	0.1304	0.1260	0.1296
$R_w(F^2)$ [$I > 2\sigma(I)$]	0.1011	0.1361	0.0966	0.2463	0.2849	0.2647	0.2659
$R_w(F^2)$ (all data)	0.1182	0.1370	0.0994	0.2927	0.3007	0.2796	0.2937
GoF	1.051	1.361	1.061	1.079	1.043	1.287	1.072

Table 2. Fe–N bond lengths and parameters for $\mathbf{1}^{\mathbf{LS-LS}}$, $\mathbf{1}^{\mathbf{LS-HS}}$, $\mathbf{1}^{\mathbf{HS-HS}}$, **2a**, $\mathbf{2b}^{\mathbf{LS}}$, $\mathbf{2b}^{\mathbf{LS/HS}}$ and $\mathbf{2b}^{\mathbf{HS}}$.

Bonds and angles	$\mathbf{1}^{\mathbf{LS-LS}}$	$\mathbf{1}^{\mathbf{LS-HS}}$	$\mathbf{1}^{\mathbf{HS-HS}}$	**2a**	$\mathbf{2b}^{\mathbf{LS}}$	$\mathbf{2b}^{\mathbf{LS/HS}}$	$\mathbf{2b}^{\mathbf{HS}}$
Fe1–N1 [Å]	1.959(3)	1.980(4)	2.094(3)	2.077(5)	2.032(6)	2.046(5)	2.091(5)
Fe1–N2 [Å]	1.998(3)	2.050(4)	2.194(3)	2.208(4)	2.135(5)	2.161(5)	2.214(4)
Fe1–N4 [Å]	2.006(3)	2.053(5)	2.233(3)	2.198(5)	2.136(5)	2.161(5)	2.225(4)
Fe2–N7 [Å]	2.073(3)	2.217(4)	2.217(3)	–	–	–	–
Fe2–N9 [Å]	2.064(3)	2.174(5)	2.210(3)	–	–	–	–
Fe2–N10 [Å]	2.007(3)	2.097(5)	2.092(3)	–	–	–	–
$\langle d_{Fe1-N} \rangle$ [Å]	1.987(3)	2.029(5)	2.173(3)	2.161(5)	2.100(5)	2.122(5)	2.176(6)
$\langle d_{Fe2-N} \rangle$ [Å]	2.047(3)	2.163(5)	2.174(3)	–	–	–	–
Σ_{Fe1} [°]	34.7	37.9	42.6	45.6	41.4	41.7	44.7
Σ_{Fe2} [°]	31.2	39.6	49.7	–	–	–	–
π–π interactions [Å]	3.947(4), 3.877(4)	4.078(2), 3.860(3)	4.297(3),3.975(2)	–	–	–	–
S···S/Se···Se interactions [Å]	–	–	–	3.638(2)	3.437(6)	3.449(8)	3.498(4)

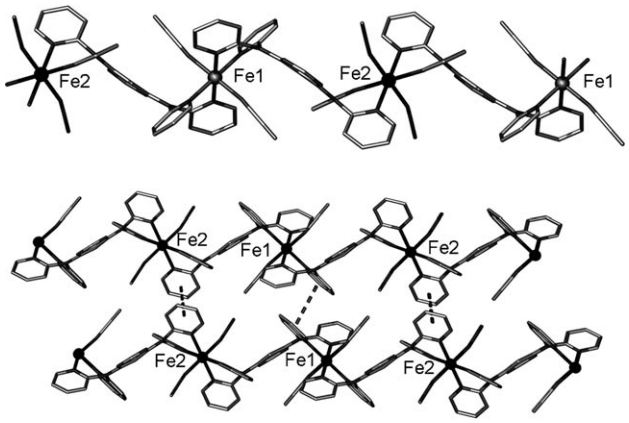

Figure 5. Illustration of 1D polymeric chains in **1** (top), where there are two distinct iron(II) centres, Fe1 and Fe2, which at 123 K are in alternating HS (black) and LS (grey) states. Illustration of the crystal packing of the 1D chains in **1** (bottom) highlighting the intermolecular π–π interactions (···) between Fe2···Fe2 and Fe1···Fe1 coordination environments. The 1D chains run along [111]. Iron(II) ions are represented as spheres and all other atoms as sticks. Hydrogen atoms have been omitted for clarity.

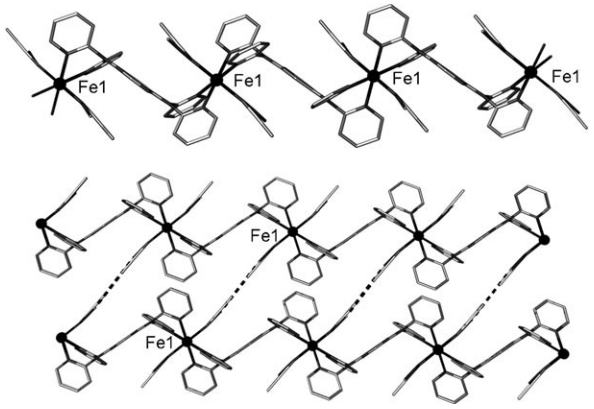

Figure 6. Illustration of the 1D polymeric chains of the isostructural materials **2a** and **2b** (top), where there is one distinct iron(II) centre, Fe1, and the S or Se atoms are disordered over two sites. Illustration of the crystal packing of the 1D chains in **2a** and **2b** (bottom) highlighting the intermolecular S···S or Se···Se interactions (···) in **2a** and **2b**, respectively. The 1D chains run along [101]. Iron(II) ions are represented as spheres and all other atoms as sticks. Hydrogen atoms have been omitted for clarity.

distinct iron(II) centres in the asymmetric unit, Fe1 and Fe2, one full bdpp ligand and one NCS^- anion bound to each iron(II) centre, the remainder generated by symmetry.

The geometries of the iron(II) centres differ significantly at 25, 123 and 250 K, highlighting the changes in spin state and subtly different crystallographic environments of Fe1 and Fe2. At 25 K, $\mathbf{1}^{\mathbf{LS-LS}}$, the $\langle d_{Fe-N} \rangle$ of Fe1 and Fe2 are 1.987(3) and 2.047(3) Å, respectively, indicative of LS iron(II). At 123 K, $\mathbf{1}^{\mathbf{LS-HS}}$, the $\langle d_{Fe-N} \rangle$ of Fe1 and Fe2 are 2.029(5) and 2.163(5) Å, respectively, indicative of Fe1 in the LS state and Fe2 in the HS state. At 250 K, $\mathbf{1}^{\mathbf{HS-HS}}$, the $\langle d_{Fe-N} \rangle$ of Fe1 and Fe2 are 2.173(3) and 2.174(3) Å, respectively, indicative of HS iron(II). Generally, large changes in the Σ values are observed over a spin transition;[25] however, here the Σ values appear to be relatively insensitive to spin state, with values of 37.9 and 39.6 ° for the $Fe1^{LS}$ and $Fe2^{HS}$ sites, respectively, at 123 K. There is, however, a notable increase in these values with increasing temperature; Σ values for Fe1 and Fe2 are 34.7 and 31.2 °, respectively, at 25 K, and 42.6 and 49.7 °, respectively, at 250 K. Accompanying these SCO-induced structural changes are an increase in the intra-chain Fe1···Fe2 separation distance from 9.156(6) Å for $\mathbf{1}^{\mathbf{LS-LS}}$ to 9.235(4) Å for $\mathbf{1}^{\mathbf{LS-HS}}$ to 9.252(5) Å for $\mathbf{1}^{\mathbf{HS-HS}}$, associated with the increase in Fe–N distances from LS to HS states.

The parallel 1D chains of **1** propagate along the [111] direction and are stacked such that there is no solvent accessible void volume (Figure 5).[18] The nearest interchain Fe2···Fe2 distances are 8.564(6), 8.721(4) and 8.969(6) Å for $\mathbf{1}^{\mathbf{LS-LS}}$, $\mathbf{1}^{\mathbf{LS-HS}}$ and $\mathbf{1}^{\mathbf{HS-HS}}$, respectively, shorter than that within the chain, highlighting the close-packed nature of these chains. Further to this, there is an array of π–π interactions between pyridyl rings on adjacent chains related by a translation along the *a*-axis (Figure 5). There are two different types of such interaction: between pyridyl rings attached to Fe1 atoms on adjacent chains or between pyridyl rings attached to Fe2 atoms on adjacent chains. The pyridyl ring centroid-to-centroid distances vary with temperature; for

Fe1 and Fe2 this distance is 3.947(4) and 3.877(4) Å, respectively, at 25 K; 4.078(2) and 3.860(3) Å at 123 K, and 4.297(3) and 3.975(2) Å at 250 K. No significant S···S interactions were observed.

*Structure of [Fe(NCS)$_2$(bdpp)] (**2a**)*: Compound **2a** has essentially the same 1D chain structure as **1**, although a different mode of packing results in a monoclinic rather than triclinic cell. In contrast to **1**, there is only one crystallographically distinct iron(II) centre at 123 K; it has an $\langle d_{Fe-N}\rangle$ of 2.161(5) Å, which is indicative of iron(II) in the HS state, and an Σ value of 45.7 °. The remaining asymmetric unit is comprised of half a bdpp ligand and one NCS^- anion for which the C and S atoms are disordered over two 50% occupied sites. The full ligand and extra NCS^- ligand are generated by symmetry.

The 1D chains in **2a** run along the [101] direction (Figure 6), with the closest Fe···Fe distance being 8.618(7) Å. The intra-chain Fe1···Fe1 separation of 9.601(5) Å is similar to that of **1**. The close packing of these chains leaves essentially no solvent accessible void volume (calculated 2.6%).[26] Between adjacent chains there are long S···S interactions, 3.638(2) Å (Figure 6), and, in direct contrast to **1**, there are no interchain π–π *?* interactions.

*Structure of [Fe(NCSe)$_2$(bdpp)] (**2b**)*: The material **2b** is isostructural to **2a**, crystallising in a monoclinic symmetry. As in **2a**, there is one crystallographically distinct iron(II) centre in the asymmetric unit, Fe1, half a bdpp ligand and one $NCSe^-$ anion where the C and Se atoms are disordered over two 50% occupied sites (**A** and **B**, Figure 7). The full ligand and extra $NCSe^-$ ligand are generated through symmetry. The 1D chains run along the [101] direction, with closest interchain Fe···Fe distances of 8.572(6), 8.608(8) and 8.648(9) Å for $\mathbf{2b^{LS}}$, $\mathbf{2b^{LS/HS}}$ and $\mathbf{2b^{HS}}$, respectively (Figure 5). They are close packed such that there is no solvent-accessible void volume.[26] As for **2a**, there are Se···Se contacts between adjacent chains of 3.437(6), 3.449(8) and 3.498(4) Å for $\mathbf{2b^{LS}}$, $\mathbf{2b^{LS/HS}}$ and $\mathbf{2b^{HS}}$, respectively (Figure 5) and no interchain π–π interactions. The positional disorder of the $NCSe^-$ ligand results in two possible Se···Se contacts between adjacent chains, that is, **A**···**B** or **B**···**A** (Figure 7). No ordering of these Se–Se interactions are apparent.

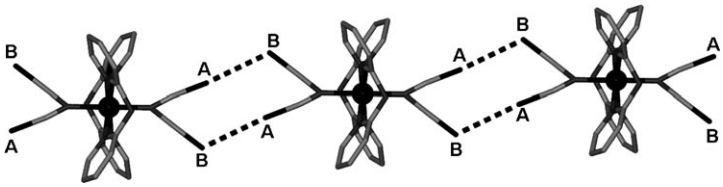

Figure 7. Representation of the **A** and **B** disorder of the $NCSe^-$ anions for **2b** and the A···B/B···A Se···Se interactions between adjacent chains. Se···Se interactions lie along both the [110] and [1−10] directions.

Structural analysis for this material at each of the temperatures was carried out in a number of lower symmetry monoclinic *C* and *P* and triclinic *P* space groups, in particular for the 150 K structure, to determine if two crystallographically distinct iron(II) centres were present, as for **1**, and to confirm that the $NCSe^-$ anion disorder observed was not due to high symmetry constrains. For all space groups and temperatures the single iron(II) centre and disordered $NCSe^-$ anions were confirmed through comparison of relevant bond lengths and site occupancies, respectively.

Most notably, diffuse scattering planes were observed in the diffraction images for the 90 and 150 K structures, but not for the 250 K structure, suggesting that long-range ordering of the iron(II) centres at these temperatures occurs in the direction of the diffuse planes (Figure 8a). The diffuse scattering planes are observed in $h0l$ with Bragg reflections where $h+l=$constant for the monoclinic *C* cell and are located exactly between these Bragg peaks. The direction and location of the diffuse planes provide evidence for long-range HS-LS-HS-LS communication along the direction of the 1D chains but a random distribution between adjacent chains (Figure 8b). No evidence for communication in the $NCSe^-$ directions ([110] and [1−10]) was found, suggesting that there is no ordering of the disordered $NCSe^-$ units between adjacent 1D chains (Figure 8b). Further to this, the absence of diffuse planes in the 250 K data suggests no ordering at this temperature. Thus, we attribute the 1D structural ordering of alternating iron(II) centres directly to lattice energy minimisation associated with the half-step HS to HS-LS crossover, a structural ordering that is retained with further cooling through the HS-LS to LS transition.

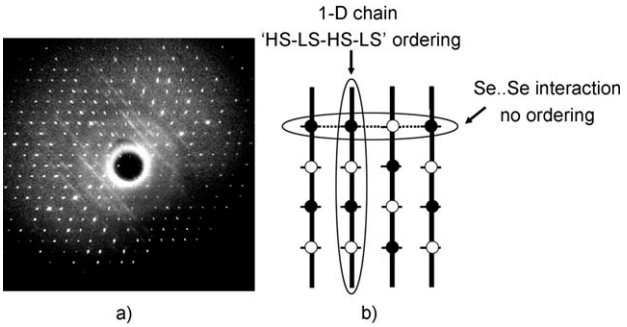

Figure 8. a) Single-crystal diffraction precession image of the $h0l$ plane at 150 K for **2b** highlighting the diffuse scattering planes, which lie exactly between the Bragg peaks. b) Schematic diagram of the "HS-LS-HS-LS" ordering of the iron(II) centres along the 1D chains ([101]) for **2b** at the intermediate plateau temperature. Highlighted also is the random ordering of adjacent iron(II) centres along the directions of Se···Se interactions ([110] and [1−10]). The HS and LS states of iron(II) centres are represented as white and black spheres, respectively. The 1D chains are represented as thick black lines and the $NCSe^-$ ligands as thin black lines.

Whilst the diffuse planes of scattering indicate 1D ordering of the iron(II) centres at 90 and 150 K, structure determination through analysis of Bragg spots at these tempera-

tures provides a model with only one unique iron(II) centre. This centre shows variation in coordination geometry at 90, 150 and 250 K which reflect the spin state changes. At 90 K, **2b**^{LS}, the $\langle d_{Fe-N}\rangle$ is 2.100(5) Å, indicative of LS iron(II). At 150 K, **2b**$^{LS/HS}$, the $\langle d_{Fe-N}\rangle$ is 2.122(5) Å, indicative of an "averaged" LS/HS iron(II) site. At 250 K, **2b**^{HS}, the $\langle d_{Fe-N}\rangle$ is 2.176(6) Å, indicative of HS iron(II). As in **1**, the Σ value is relatively insensitive to the spin state, with values of 41.4, 41.7 and 44.7 ° at 90, 150 and 250 K, respectively. Additionally, the interchain Fe···Fe separations show a general increase from LS to HS states, with values of 9.554(6), 9.587(7) and 9.642(4) Å for **2b**^{LS}, **2b**$^{LS/HS}$ and **2b**^{HS}, respectively.

Discussion

There are a number of points regarding the SCO phenomenon that this series of materials present: the occurrence of a spin transition in polymorphic and isomorphic materials, structure-property relationships in two-step spin transitions, and light-induced spin state trapping in polymeric materials. Each of these aspects are of current interest to the wider magnetic community, particularly towards identifying structurally ordered versus disordered intermediate states within materials displaying two-step spin transitions. Here, where we see, to the best of our knowledge, the first case of a two-step SCO in a 1D polymeric material, the opportunity arises to compare our findings with those previously reported on dinuclear (and to a lesser extent mononuclear) materials displaying two-step spin transitions.

Firstly, we discuss the observed difference in properties of the polymorphs **1** and **2a**, the former being SCO active and latter inactive despite very similar iron(II) bond lengths and octahedral distortion parameters for each compound (Table 2). There have been many reports of polymorphic materials with diverse symmetries displaying different SCO behaviours.[3,27,28] For example, three polymorphic forms of the material [Fe(dppa)(NCS)$_2$] (dppa = 3-aminopropylbis(2-pyridylmethyl)amine), **A**, **B** and **C**, show markedly different SCO behaviours; **A** shows a gradual transition, **B** remains HS to low temperature, and **C** exhibits a very abrupt transition with hysteresis.[28] The increased cooperativity in **C** compared to **A** was attributed to an array of intermolecular contacts in the crystal lattice and the lack of SCO in **B** to an elongation of Fe–N distances through strain in the crystal packing. Here, the array of π–π interactions observed in **1**, which are not observed in **2a**, likely play a role in stabilising the LS state.[3,22] The observation of SCO in **2b**, which is isostructural to **2a** and has comparable iron(II) bond lengths and octahedral distortion, may be attributed principally to the increased ligand field of the $NCSe^-$ ligand over that of NCS^-. We observed this same phenomenon in a related 1D series of materials where the $NCSe^-$ analogue also lacked inter-molecular interactions but still displayed a spin transition.[22] A further notable difference between the two structures is the existence of a series of short Se···Se interactions between adjacent chains in **2b**; Although analogous S···S interactions are observed in **2a**, they are significantly longer.

Now turning to the two-step nature of the spin transitions observed in **1** and **2b** in which there is continued interest, at a fundamental level, in the occurrence of two-step spin transitions in mono- and di-nuclear materials and the structural consequences at the IP temperature. The observation of a two-step SCO is relatively uncommon for polymeric systems and is usually observed as "averaged" HS/LS SCO sites at the IP temperature or two crystallographically distinct metal centres over all temperatures.[7,14,15,17] The 3D compound [Fe(btr)$_3$][(ClO$_4$)$_2$] provides one such example; it shows a two-step SCO ($T_{1/2(1)}$ = 184 and $T_{1/2}$ = 222 K) in which two distinct iron(II) sites exist at all temperatures and undergo a HS-HS→HS-LS→LS-LS spin state conversion.[7] In contrast, the 2D coordination polymer [Fe(py)$_2${Ag(CN)$_2$}$_2$], which also undergoes a two-step SCO, was reported to contain only one crystallographically distinct iron(II) site over the entire temperature range.[17] To our knowledge there are no reports of polymeric SCO materials that have two-step spin transitions originating from a crystallographic phase change. However, examples of mononuclear materials exist where a lowering of symmetry at the IP temperature results in distinct HS and LS sites at this point.[18,19]

In the present systems, the two-step behaviour in **1** can be directly related to the two differing iron(II) environments over all temperatures where, notably, in the completely LS (25 K) and HS (250 K) states the $\langle d_{Fe-N}\rangle$ and Σ values for Fe1 and Fe2 differ in magnitude. Hence one of the iron(II) centres in the purely HS (250 K) and LS (25 K) states undergoes a spin transition before the other to give an intermediate HS-LS structure (123 K) that contains alternating HS and LS sites. Although this is a common observation for two-step SCO materials in general, this is the first time it has been observed in a 1D polymeric complex. This result is analogous to the two-step SCO transition observed in the dinuclear system [Fe$_2$(ddpp)$_2$(NCS)$_4$]·4 CH$_2$Cl$_2$.[10]

The two-step SCO behaviour in **2b** is somewhat more interesting, with the high temperature step being concomitant with and appearing to drive a low-dimensional structural transition. Although only one distinct iron(II) site is observed through structure determination by Bragg analysis at each of the three spin state plateaux, diffuse scattering planes in (h 0 l) in the IP region clearly indicate the presence of long-range ordering in the direction of the 1D chains with a periodicity double that of the chain repeat unit. This strongly suggests that the HS-LS state in the IP region exists as alternating HS-LS-HS-LS sites along the chains. We note that the observation of 1D ordering of alternating HS-LS sites most likely originates from the steric requirements of the chains although may also arise due to anticooperative electronic interactions through the ligand; the existence of the latter is generally inconsistent, however, with a broader intermediate plateau in **2b** versus that in **1**. The lack of further diffuse scattering (or indeed additional superstructure reflections), for example in the (0 k l) and (h k 0) planes, discounts long-range ordering between adjacent chains. Nota-

bly, planes of diffuse scattering have similarly been observed in 1D charge-transfer salts that undergo charge density wave transitions driven by their electronic instability.[29] We are unaware, however, of any other reports of SCO systems where the observation of diffuse scattering provides such evidence of low dimensional long-range ordering. Most notably, in the re-investigation of $[\{Fe^{II}(2\text{-pic})_3\}Cl_2]\cdot EtOH$, which displays a classical two-step SCO, detailed inspection of X-ray diffraction images although searching for the presence of short-range correlations revealed superstructure reflections indicative of 3D long-range symmetry lowering, rather than the expected diffuse scattering.[18]

The retention of the planes of diffuse scattering in **2b** with further cooling to the fully LS state is a point of considerable interest. Although there are examples of "re-entrant" two-step SCO materials where the HS and LS states are the same symmetry but differ from the IP state, there are none that show this character.[18] The fact that the 1D structural distortion is retained in the absence of alternating HS-LS sites may reflect a degree of kinetic trapping following conversion to the fully LS state (i.e. structural memory of the "frozen-in" of the 1D ordered HS-LS-HS-LS state), but may also suggest that this perturbation is favoured thermodynamically at low temperature purely through steric interactions within the chains. Accordingly, further work is required to determine the driving force(s) for this perturbation. As there are no other 1D chain materials that undergo a two-step spin transition, this result cannot be compared, but certainly is unique among even mononuclear and dinuclear systems.

Light irradiation of **1** and **2b** at low temperature leads to the trapping of a significant fraction of iron(II) centres in the metastable HS state. Although extensive LIESST studies have been performed on mononuclear iron(II) species, few have been reported for polymeric systems.[30,31] Thus, such studies are important to determine the fundamental effect of incorporating light-initiated SCO centres into polymers. Further to this, comparison of the thermal and photo-induced SCO properties of a large number of materials has seen trends emerge regarding the relationship between the T(LIESST) (the temperature at which the light induced HS information is erased) and the $T_{1/2}$ values, such that $T(\text{LIESST}) = T_0 - 0.3T_{1/2}$.[24] Although the origin of these values is not entirely clear, the magnitude appears to be related to the rigidity and density of the ligands surrounding the iron(II) centre.[24] These studies reveal four distinct T_0 families dependent on the geometry and rigidity of ligands around the iron(II) centre: 100 K for monodentate ligands,[32] 120 K for bidentate ligands,[32] 150 K for meridional tridentate ligands,[33] and 200 K for three-dimensional network solids.[34] The materials reported here are polymeric and contain a bidentate ligand, thus their placement within these families is somewhat ambiguous, but they may be expected to lie in the $T_0 = 120$ K family for materials containing bidentate ligands.[24,32] The calculated T_0 values for **1** and **2b** are 95.5 and 109 K, respectively, based on their $T_{1/2(1)}$ values, and 82 and 86.5 K, respectively, based on their $T_{1/2(2)}$ values. This places these compounds approximately in the $T_0 = 100$ K family for the upper limit for monodentate ligands.[24] However, the binding of the dpa portion of the bdpp ligand to the iron(II) centres results in a large chelating ring due to the amine group separating the 2-pyridyl rings; thus, a degree of flexibility is anticipated such that they act essentially in a monodentate environment. Such an effect has been observed previously for the mononuclear material $[Fe(picpzpz)_2](BF_4)\cdot 2MeOH$ (picpzpz = 2-(1-pyridin-2-ylmethyl-1*H*-pyrazol-3-yl)pyrazine)), where the meridional picpzpz ligand possesses a flexible unsaturated carbon atom,[35] and the same conclusion was obtained by investigating the photomagnetic properties of iron(II) α,ω-bis(tetrazole-1-yl)alkane coordination polymers.[31] This emphasises that the vibrational aspects and hardness of the inner coordination sphere are key factors in stabilising the metastability of the light induced HS state.[24,36]

Upon quench cooling of the samples there was an observed 43.5% HS trapping at low temperatures for **1** and essentially no trapping for **2b**. The fraction of HS trapping for **1** with light irradiation is larger than that attained with thermal quench cooling, suggesting a competition between relaxation and excitation energies, where the extra energy contribution provided by the light irradiation allows a larger $\chi_M T$ value to be obtained. The absence of any trapping upon quench cooling for **2b** suggests an even greater competition between relaxation and excitation energies, where the energy contribution from the light source may not be sufficient to maintain a trapped HS fraction. Moreover, in regard to the higher $T_{1/2}$ temperature of this material (versus **1**), we could expect a lower temperature at which the light induced HS state is erased, that is, the T(LIESST) value.[24] Indeed, the calculated T(LIESST) values of 55 and 49 K for **1** and **2b**, respectively, are consistent with this conclusion.

Conclusion

A series of 1D chain materials of the general formula, $[Fe(NCX)_2(bdpp)]$ in which X = S or Se, have been synthesised and the SCO behaviours characterised magnetically (both thermal and light-induced) and structurally. This study has provided a unique insight into the influence of polymorphism and axial ligand variation on SCO and fundamental examples of the diverse structural consequences possible in a two-step SCO. Notably, these are the first 1D polymeric materials that undergo two-step spin transitions.

The thiocyanate containing materials **1** and **2a** are polymorphs with vastly different magnetic behaviours: **1** displays a full two-step SCO ($T_{1/2} = 135$ and 90 K) and **2a** remains HS over all temperatures. This difference can be attributed to differences in crystal packing, most notably to an array of inter-molecular π–π interactions in **1**, which are absent in **2a**. In contrast, the selenocyanate analogue, **2b**, is isostructural to **2a** and displays a full two-step SCO ($T_{1/2} = 200$ and 125 K) owed, in part, to the stronger ligand field imparted by selenocyanate over that of thiocyanate. The structural

and magnetic comparisons made here highlight the subtle balance between ligand field strength and inter-molecular interaction on the SCO phenomenon.

Structural analysis of **1** reveals two crystallographically distinct iron(II) sites over all temperatures, with the structure in the IP region containing alternating LS and HS sites along the 1D chains. This is a rare observation in polymeric SCO materials, the most commonly observed case being an "averaged" LS/HS site. In marked contrast, although we observe only one distinct crystallographic iron(II) site for **2b** over the three plateau regions with an "averaged" LS/HS state in the IP region, the presence of diffuse scattering planes indicates long-range ordering of alternating HS-LS iron(II) along the 1D chains. As such, we assign this compound to the even more rare class of two-step SCO materials in which crossover drives a symmetry-lowering phase transition. The fact that this transition is low-dimensional, and therefore only observable crystallographically through analysis of diffuse scattering, highlights the fact that further structural analysis of other two-step SCO systems with apparently "averaged" IP structures is warranted. Interestingly, the 1D structural perturbation is retained at low temperature in the fully LS state (90 K). These two contrasting examples within one chemical series provide novel insight into structure-property relationships for the two-step SCO phenomenon. Notably, the observation of a broader intermediate plateau in **2b** compared to that of **1** suggests that steric considerations rather than anticooperative electronic interactions between alternating intrachain HS-LS sites principally determine the two-step behaviour.

Significant trapping of a HS metastable species with green light irradiation for both **1** and **2b** is observed (i.e. the LIESST effect). Notably, comparison of the observed $T_{1/2}$ and T(LIESST) values for these materials (using the trend $T(\text{LIESST}) = T_0 - 0.3T_{1/2}$) places them with materials containing monodentate ligands, despite their containing bidentate ligands. The large chelate ring of the dpa ligand provides a degree of flexibility, making it a less rigid bidentate in regards to its photomagnetic memory. This highlights the outer coordination sphere considerations that must be considered for light-induced magnetism. Relaxation kinetics measured on the HS fraction of **2b**, formed after laser irradiation at 10 K, fitted well to a stretched exponential model and were in agreement with low cooperativity in this 1D system.

Experimental Section

All chemicals were obtained from Aldrich and Fluka and used without further purification.

Ligand synthesis: A mixture of 4,6-dichloropyrimidine (1.51 g, 10 mmol), 2,2-dipyridylamine (3.5 g, 20 mmol), sodium carbonate (2 g), copper powder (0.05 g), potassium bromide (trace) and mesitylene (5 mL) were heated at 160 °C for 5 days. The mesitylene was then removed in vacuo. The resultant brown product was dissolved in dichloromethane and filtered. The filtrate was then taken to dryness *in vacuo* and the resulting oil purified on a silica gel column (20×5 cm) eluting with 1:40 methanol-chloroform solution. The second fraction was collected, washed with cold ethyl acetate and recrystallised from ethanol-ether to give a pale yellow solid (yield 0.98 g, 20%). m.p. 192–194 °C; ^{1}H NMR ($CDCl_3$) $\delta = 8.52$ (s, 1H), 8.42 (dd, 4H), 7.71 (t, 4H), 7.26 (d, 4H), 7.14 (dd, 4H), 6.51 ppm (s, 1H); ^{13}C NMR ($CDCl_3$) $\delta = 162.5$, 158.2, 155.9, 149.0, 138.0, 120.9, 120.7, 99.2 ppm; ES-MS 419.2 $[(M+1)]^+$; elemental analysis calcd (%) for $C_{24}H_{18}N_8$: C 68.89, H 4.34, N 26.78; found: C 69.00, H 4.49, N 26.81.

Synthesis of [Fe(NCS)$_2$(bdpp)] (1 and 2a): A solution of bdpp (30 mg, 0.1 mmol) in methanol (2 mL) was placed at the base of one arm of an H-shaped tube. A solution of $[Fe(ClO_4)_2]\cdot 6H_2O$ (18.6 mg, 0.1 mmol) and NaNCS (12.0 mg, 0.2 mmol) in methanol (2 mL) was placed in the other arm of the H-shaped tube. Solvent methanol was carefully layered to fill the rest of the tube, which was then stoppered. After two weeks a mixture of yellow block crystals of **1** and bright yellow rectangular rod crystals of **2a** formed (yield: 50 mg composed of **1** ≈25%, **2a** ≈75%). Owing to the distinct variation in colour and morphology, separation of the two crystalline forms for magnetic studies was achieved easily. Attempts to vary the solvent system and relative concentrations of the reactants to produce single phase samples were found to not affect the relative ratios of **1** and **2a** formed. IR (mixture of **1** and **2a**): $\tilde{\nu} = 2056$(s), 1608 (m), 1554(m), 1461(s), 1416(s), 1264(w), 1230 cm^{-1} (w); elemental analysis calcd (%) for $C_{26}H_{18}FeN_{10}S_2$: C 52.89, H 3.07, N 23.72; found: C 51.60, H 3.26, N 23.32.

Synthesis of [Fe(NCSe)$_2$(bdpp)] (2b): A solution of bdpp (30 mg, 0.1 mmol) in methanol (2 mL) was placed at the base of one arm of an H-shaped tube. A solution of $[Fe(ClO_4)_2]\cdot 6H_2O$ (18.6 mg, 0.1 mmol) and KNCSe (20.6 mg, 0.2 mmol) in methanol (2 mL) was placed in the other arm of the H-shaped tube. Methanol was again carefully layered to fill the rest of the tube, which was then stoppered. After two weeks yellow rectangular rod crystals formed (yield: 25 mg, 51%). IR (**2b**): $\tilde{\nu} = 2052$(s), 1604(m), 1548(m), 1462(s), 1410(s), 1263(w), 1230 cm^{-1} (w); elemental analysis calcd (%) for $C_{26}H_{18}FeN_{10}Se_2$: C 45.64, H 2.65, N 20.47; found: C 44.53, H 2.67, N 20.09.

Magnetic susceptibility: Magnetic susceptibility data were collected using a Quantum Design MPMS-5 Quantum design SQUID magnetometer under an applied field of 1 T over the temperature range 4–250 K. Polycrystalline samples of **1**, **2a** and **2b** were placed in gel capsules held within plastic straws. A standard measurement involved slow cooling of the sample to 4 K, heating to 250 K and cooling under the same conditions. Additional measurements were carried out for **1** and **2b** were the sample was quench-cooled from room temperature to 4 K. Torquing of crystallites was observed for the polycrystalline sample of **2b** so further measurements were carried out with samples dispersed in a Vaseline mull and subsequently placed in gel capsules. Care was taken for each of these measurements to allow long thermal equilibration times at each temperature point.

Photomagnetic characterisation for **1** and **2b** was carried out using a Kr^+ laser coupled through an optical fibre into the cavity of the a MPMS-55 Quantum design SQUID magnetometer operating at 2 T. Samples were prepared as a thin layer (≈0.1 mg) to promote full penetration of the irradiated light. The sample weight was obtained by comparing its thermal spin transition behaviour with a heavier and accurately weighed sample.[24] The sample was first slow cooled to 10 K, ensuring that potential trapping of HS species at low temperatures did not occur. Irradiation to photo-saturation was carried out a number of times using different wavelengths (i.e. 337/356.4 nm; 406.7/415.4 nm; 530.2 nm; 647.1/676.4 nm and 752.5/799.3 nm) to determine which source was most efficient and power intensity up to 5 mW cm^{-2}. The sample in the LS state was then irradiated with green light ($\lambda = 530.2$ nm at 5 mW cm^{-2}), the most efficient, until photosaturation was reached. Then, in the absence of irradiation, the temperature was increased at 1 K steps to 100 K, to determine the T(LIESST) value, and 3 K steps over the range 100–300–10 K, to follow the thermal spin transition. The extreme of the $\partial\chi_M T/\partial T$ versus T plot gave the T(LIESST) value, defined as the temperature for which the light induces HS information is erased.[24] At 10 K, the sample **2b** was again irradiated to photo-saturation and, in the absence of irradiation and the relaxation kinetics at 10, 40, 46, 50 and 55 K were measured (see the Supporting Information).

Crystallographic data collection and refinement: Single-crystal data for $\mathbf{1}^{\mathbf{LS-HS}}$, $\mathbf{1}^{\mathbf{HS-HS}}$, **2a**, $\mathbf{2b}^{\mathbf{LS}}$, $\mathbf{2b}^{\mathbf{LS/HS}}$ and $\mathbf{2b}^{\mathbf{HS}}$ were collected on a Bruker APEX X8 diffractometer equipped with graphite-monochromated $Mo_{K\alpha}$ radiation ($\lambda = 0.7017$ Å) and an Oxford Instruments Nitrogen Cryostream. Single-crystal data for $\mathbf{1}^{\mathbf{LS-LS}}$ were collected on a Bruker SMART 1000 CCD using $Mo_{K\alpha}$ radiation ($\lambda = 0.7017$ Å) and an HELIX helium gas cryostream. Single crystals were mounted on either a MiTeGen MicroMounts fibre or a mohair fibre using oil. Data collection for the structures of $\mathbf{1}^{\mathbf{LS-HS}}$ (123 K) and $\mathbf{1}^{\mathbf{HS-HS}}$ (250 K) were carried out on the same crystal, a different crystal was used for the 25 K structure ($\mathbf{1}^{\mathbf{LS-LS}}$). Similarly, data collection for the structures of $\mathbf{2b}^{\mathbf{LS}}$ (90 K) and $\mathbf{2b}^{\mathbf{HS}}$ (250 K) were carried out on the same crystal, a different crystal was used for the 150 K structure ($\mathbf{2b}^{\mathbf{LS/HS}}$). Diffraction data analysis and reduction were performed within SMART and SAINT+.[37] Corrections for Lorenz, polarisation and absorption effects were performed within SADABS.[38] Structures were solved using a combination of direct and Patterson methods within SHELXS-97 and refined using SHELXL-97 within X-SEED.[39] CCDC 667864 ($\mathbf{1}^{\mathbf{HS-HS}}$), 667865 ($\mathbf{1}^{\mathbf{LS-HS}}$), 667866 ($\mathbf{1}^{\mathbf{LS-LS}}$), 667867 (**2a**), 667868 ($\mathbf{2b}^{\mathbf{HS}}$), 667869 ($\mathbf{2b}^{\mathbf{LS}}$) and 667870 ($\mathbf{2b}^{\mathbf{LS/HS}}$) contain the supplementary crystallographic data for this paper. These data can be obtained free of charge from The Cambridge Crystallographic Data Centre via www.ccdc.cam.ac.uk/data_request/cif.

Acknowledgements

The Australian Research Council, ARC, is thanked for providing a Discovery Grant to support this work. Financial support for the photomagnetic LIESST work was kindly provided by a French–Australia FAST/DEST grant and this allowed the Australian participants to travel to Bordeaux to carry out measurements. The authors would also like to thank the Aquitaine Region for supporting the development of the international platform of photomagnetism.

[1] P. Gütlich, H. A. Goodwin, *Top. Curr. Chem.* **2004**, *233*, 1.
[2] O. Kahn, *Molecular Magnetism*, VCH, New York, **1993**.
[3] J.-F. Létard, P. Guionneau, L. Goux-Capes, *Top. Curr. Chem.* **2004**, *235*, 221.
[4] K. S. Murray, C. J. Kepert, *Top. Curr. Chem.* **2004**, *233*, 195.
[5] Y. Garcia, V. Niel, C. Muñoz, J. A. Real, *Top. Curr. Chem.* **2004**, *233*, 229; E. Breuning, M. Ruben, J. M. Lehn, F. Renz, Y. Garcia, V. Ksenofontov, P. Gütlich, E. Wegelius, K. Rissanen, *Angew. Chem.* **2000**, *112*, 2563; *Angew. Chem. Int. Ed.* **2000**, *39*, 2504.
[6] J. Krober, J. P. Audiere, R. Claude, E. Codjovi, O. Kahn, J. G. Haasnoot, F. Groliere, C. Jay, A. Bousseksou, J. Linares, F. Varret, A. Gonthiervassal, *Chem. Mater.* **1994**, *6*, 1404; O. Kahn, C. J. Martinez, *Science* **1998**, *279*, 44; V. Niel, J. M. Martinez-Agudo, M. C. Muñoz, A. B. Gaspar, J. A. Real, *Inorg. Chem.* **2001**, *40*, 3838.
[7] Y. Garcia, O. Kahn, L. Rabardel, B. Chansou, L. Salmon, J. P. Tuchagues, *Inorg. Chem.* **1999**, *38*, 4663.
[8] V. Niel, M. C. Muñoz, A. B. Gaspar, A. Galet, G. Levchenko, J. A. Real, *Chem. Eur. J.* **2002**, *8*, 2446.
[9] J. A. Real, E. Andres, M. C. Muñoz, M. Julve, T. Granier, A. Bousseksou, F. Varret, *Science* **1995**, *268*, 265; N. Moliner, C. Muñoz, S. Letard, X. Solans, N. Menendez, A. Goujon, F. Varret, J. A. Real, *Inorg. Chem.* **2000**, *39*, 5390; G. J. Halder, C. J. Kepert, B. Moubaraki, K. S. Murray, J. D. Cashion, *Science* **2002**, *298*, 1762; S. M. Neville, B. Moubaraki, K. S. Murray, C. J. Kepert, *Angew. Chem.* **2007**, *119*, 2105; *Angew. Chem. Int. Ed.* **2007**, *46*, 2059.
[10] J. J. Amoore, C. J. Kepert, J. D. Cashion, B. Moubaraki, S. M. Neville, K. S. Murray, *Chem. Eur. J.* **2006**, *12*, 8220.
[11] A. B. Gaspar, V. Ksenofontov, V. Martinez, M. C. Muñoz, J. A. Real, P. Gütlich, *Eur. J. Inorg. Chem.* **2004**, 4770; V. Ksenofontov, A. B. Gaspar, V. Niel, S. Reiman, J. A. Real, P. Gutlich, *Chem. Eur. J.* **2004**, *10*, 1291; B. A. Leita, B. Moubaraki, K. S. Murray, J. P. Smith, J. D. Cashion, *Chem. Commun.* **2004**, 156; S. Brooker, P. G. Plieger, B. Moubaraki, K. S. Murray, *Angew. Chem.* **1999**, *111*, 424; *Angew. Chem. Int. Ed.* **1999**, *38*, 408; K. Nakano, S. Kawata, K. Yoneda, A. Fuyuhiro, T. Yagi, S. Nasu, S. Morimoto, S. Kaizaki, *Chem. Commun.* **2004**, 2892.
[12] M. H. Klingele, B. Moubaraki, J. D. Cashion, K. S. Murray, S. Brooker, *Chem. Commun.* **2005**, 987.
[13] V. Ksenofontov, A. B. Gaspar, J. A. Real, P. Gütlich, *J. Phys. Chem. B* **2001**, *105*, 12266; M. Yamada, M. Ooidemizu, Y. Ikuta, S. Osa, N. Matsumoto, S. Iijima, M. Kojima, F. Dahan, J. P. Tuchagues, *Inorg. Chem.* **2003**, *42*, 8406.
[14] M. C. Muñoz, A. B. Gaspar, A. Galet, J. A. Real, *Inorg. Chem.* **2007**, *46*, 8182.
[15] C. M. Grunert, J. Schweifer, P. Weinberger, W. Linert, K. Mereiter, G. Hilscher, M. Muller, G. Wiesinger, P. J. van Koningsbruggen, *Inorg. Chem.* **2004**, *43*, 155.
[16] G. S. Matouzenko, D. Luneau, G. Molnar, N. Ould-Moussa, S. Zein, S. A. Borshch, A. Bousseksou, F. Averseng, *Eur. J. Inorg. Chem.* **2006**, 2671.
[17] J. A. Rodriguez-Velamazan, M. Castro, E. Palacios, R. Burriel, T. Kitazawa, T. Kawasaki, *J. Phys. Chem. B* **2007**, *111*, 1256.
[18] D. Chernyshov, M. Hostettler, K. W. Törnroos, H. B. Bürgi, *Angew. Chem.* **2003**, *115*, 3955; *Angew. Chem. Int. Ed.* **2003**, *42*, 3825.
[19] D. L. Reger, C. A. Little, V. G. Young and P. Maren, *Inorg. Chem.*, **2001**, *40*, 2870; K. W. Törnroos, M. Hostettler, D. Chernyshov, B. Vangdal, H. B. Bürgi, *Chem. Eur. J.* **2006**, *12*, 6207.
[20] A. B. Gaspar, G. Agusti, V. Martinez, M. C. Muñoz, G. Levchenko, J. A. Real, *Inorg. Chim. Acta* **2005**, 4089.
[21] M. Quesada, M. Monrabal, G. Aromí, V. A. Peña-O'Shea, M. Gich, E. Molins, O. Roubeau, S. Teat, E. MacLean, P. Gamez, R. J. , *J. Mater. Chem.* **2006**, *26*, 2669.
[22] S. M. Neville, B. A. Leita, D. A. Offermann, M. B. Duriska, B. Moubaraki, K. W. Chapman, G. J. Halder, K. S. Murray, *Eur. J. Inorg. Chem.* **2007**, 1073.
[23] M. Quesada, V. A. Pena-O'Shea, G. Aromi, S. Geremia, C. Massera, O. Roubeau, P. Gamez, J. Reedijk, *Adv. Mater.* **2007**, *19*, 1397.
[24] J.-F. Létard, *J. Mater. Chem.* **2006**, *16*, 2550.
[25] P. Guionneau, M. Marchivie, G. Bravic, J.-F. Létard, D. Chasseau, **2004**, *234*, 97.
[26] A. L. Spek, *Platon. A multipurpose crystallography tool*, Utrecht University, The Netherlands, **2000**.
[27] E. König, K. Madeja, *Inorg. Chem.* **1967**, *6*, 48; E. König, K. Madeja, K. J. Watson, *J. Am. Chem. Soc.* **1968**, *90*, 1146; M. Marchivie, P. Guionneau, J.-F. Létard, D. Chasseau, *Acta Cryst. B.* **2003**, *59*, 479; A. Ozrowski, B. R. McGarvey, A. B. Sarkar, J. E. Drake, *Inorg. Chem.* **1988**, *27*, 627.
[28] G. S. Matouzenko, A. Bousseksou, S. Lecocq, J. P. van Koningsbruggen, M. Perrin, O. Kahn, A. Collet, *Inorg. Chem.* **1997**, *36*, 5869.
[29] R. Comes, M. Lambert, H. Launois, H. R. Zeller, *Phys. Rev. B* **1973**, *8*, 572.
[30] A. Hauser, *Top. Curr. Chem.* **2004**, *234*, 155.
[31] A. Absmeier, M. Bartel, C. Carbonera, G. N. L. Jameson, P. Weinberger, A. Caneschi, K. Mereiter, J.-F. Létard, W. Linert, *Chem. Eur. J.* **2006**, *12*, 2235; A. Absmeier, M. Bartel, C. Carbonera, G. N. L. Jameson, F. Werner, M. Reissner, A. Caneschi, J.-F. Létard, W. Linert, *Eur. J. Inorg. Chem.* **2007**, 3047.
[32] J.-F. Létard, L. Capes, G. Chastanet, N. Moliner, S. Létard, J. A. Real, O. Kahn, *Chem. Phys. Lett.* **1999**, *313*, 115.
[33] C. Carbonera, J. S. Costa, V. A. Money, J. Elhaúk, J. A. K. Howard, M. A. Halcrow, J.-F. Létard, *Dalton Trans.* **2006**, 3058; S. Marcén, L. Lecren, L. Capes, H. A. Goodwin, J.-F. Létard, *Chem. Phys. Lett.* **2002**, *358*, 87.
[34] N. Shimamoto, S.-S. Ohkoshi, O. Sato, K. Hashimoto, *Inorg. Chem.* **2002**, *41*, 678.
[35] B. A. Leita, S. M. Neville, G. J. Halder, B. Moubaraki, C. J. Kepert, J.-F. Létard, K. S. Murray, *Inorg. Chem.* **2007**, *46*, 8784.
[36] J.-F. Létard, P. Guionneau, O. Nguyen, J. S. Costa, S. Marcén, G. Chastanet, M. Marchivie, L. Goux-Capes, *Chem. Eur. J.* **2005**, *11*, 4582; S. Bonhommeau, N. Brefuel, V. K. Palfi, G. Molnar, A. Zwick,

L. Salmon, J.-P. Tuchagues, J. S. Costa, J.-F. Létard, H. Paulsen, A. Bousseksou, *Phys. Chem. Chem. Phys.* **2005**, *7*, 2909.
[37] *SMART*, *SAINT and XPREP.* Area detector and data integration and reduction software, Bruker Analytical Instruments Inc., Madison, Wisconsin, USA, **1995**.
[38] G. M. Sheldrick, *SADABS.* Empirical adsorption correction program for area detector data, University of Gottingen, Germany, **1996**.
[39] *SHELXL97. Program for crystal structural solution and refinement*, Bruker Analytical Instruments Inc., Madison, Wisconsin, USA, **1997**; L. J. Barbour, *X-SEED*, University of Stellenbosch, South Africa, **1999**.

Received: May 9, 2008
Published online: September 18, 2008

